IEEE Access
Multidisciplinary | Rapid Review | Open Access Journal

Received January 27, 2022, accepted March 21, 2022, date of publication March 28, 2022, date of current version April 7, 2022.

Digital Object Identifier 10.1109/ACCESS.2022.3162903

Design and Analysis of Flexure Mechanisms for Human Hand Tremor Compensation

MOHAMMAD ZUBAIR, (Graduate Student Member, IEEE), BHIVRAJ SUTHAR, (Graduate Student Member, IEEE), AND SEUL JUNG, (Member, IEEE)
Mechatronics Engineering Department, Chungnam National University, Daejeon 34134, South Korea

Corresponding author: Seul Jung (jungs@cnu.ac.kr)

This work was supported by the National Research Foundation (NRF) of Korea under Grant 2017K1A3A1A68072072 and Grant 2019R1I1A3A01062567.

ABSTRACT Tremor is an involuntary action and a common problem for elderly people and other age groups to perform daily activities. To assist those people in conducting daily activities, suppressing hand tremors is necessary. A flexure mechanism system can be placed as a tabletop device on which the elbow can be positioned to compensate for the tremor. Using this methodology, in this paper, flexure-based mechanisms for the hand tremor are proposed to help people perform eating activities easily. Flexure mechanisms with three different connection arrangements are designed, modeled (as pseudo-rigid bodies), analyzed, and developed. Finite element analysis is conducted to verify the results of the pseudo-rigid models for passive conditions. An experimental setup is accessed for both passive and active schemes, consisting of two link mechanisms, having a precise one-DOF tremor generated at the end-effector of the experimental setup arm. Gyroscope sensors are used to monitor the tremor present. A series of experiments are conducted for two cases: when flexure mechanisms are connected passively and when flexure mechanism is connected actively. It was found that the flexure mechanism can compensate for the tremor in passive and active mode by approximately 75% to 90%, respectively.

INDEX TERMS Curved flexure, hand tremor, pseudo-rigid model, passive and active tremor compensation.

I. INTRODUCTION

Hand tremor is one of the oldest symptoms and can be traced down to over hundreds of years [1]–[5]. It is an involuntary action that causes jittering of hand and makes a person incapable of doing daily activities [6], [7].

Tremor can occur in all ages due to central neurogenic and/or mechanical reflex. The nature of tremor can be of three types: normal (unequivocally), mild, and advanced tremor [8], [9]. The tremor study based on autopsy is challenging to comprehend. So, the study in general, is based on an electro-physiologic technique [9]. The frequency (ω) of tremor due to mechanical reflex can be formulated as, $\omega = \sqrt{(K/I)}$ where the known moment of inertia (I) of the arm and stiffness (K) for the joint can be used to determine the frequency of mechanical reflex of tremor [10]. Since the behavior of neurogenic reflex is difficult to be modelled, studies are carried out using sensor data and EMG signals to determine the frequency. For the severe tremor case, the frequency is known as 6 to 9 Hz [11].

Researchers have tried to develop methods to suppress the tremor. Clinicians have been attempting neuro-surgical procedures to suppress the tremor [12], but the risk to life and health has restricted patients from opting. Hand-held devices were developed to suppress tremor and enhance the capability of a person to perform daily activity [13]–[15].

In other areas, suppressing tremors during conducting surgery has been a concern for a very long time. With the advancement in a robot-based surgery, the hand tremor can be successively suppressed to travel onto the remote robot which performs the microsurgery [16], [17]. A hand-held tremor compensation device based on a piezoelectric actuator was designed to conduct microsurgery [18]. But conducting surgery using sophisticated devices needs expertized techniques, whereas hand-held surgery is more intuitive where natural feeling and force feedback are retained. The tremor can also be suppressed during microsurgery by keeping the

The associate editor coordinating the review of this manuscript and approving it for publication was Tao Liu.

arm on a resting surface, of which concept motivates our research [19].

To study the dynamics of hand tremor, a mathematical model of an arm is required, which can be carried out by the theories of robotics. An arm is considered from the shoulder to the hand and typically has three joints, i.e., a shoulder, an elbow, and a wrist joint. Many researchers have conducted the study to develop the mathematical model of the human arm [20]. The kinematics of the human arm using a position sensor in order to develop an orthosis to support the human upper arm was studied in [21]. An apparatus containing a transducer to measure elbow and shoulder forces/torques for tetraplegia patients was developed [22]. A supervised arm dynamics using an industrial robot was also studied [23], where a guided arm motion was given to determine the joint force and torque. A mathematical model to investigate the computational problem of the inverse kinematics of an eight-DOF arm model was developed [23], and the dynamics of the lower arm using the Euler- Lagrange formulation was studied [24].

In this paper, three different flexure mechanisms are proposed, modeled as pseudo-rigid bodies, and validated by using finite element analysis. Flexures are connected in combination of parallel and series arrangements to make three types of flexures.

An experimental setup is developed to test the effectiveness of the flexure mechanism to compensate for the tremor. For the experimental setup, a 2-DOF arm model is developed. The tremor on the end effector is generated using a slider-crank mechanism. The amplitude of the tremor is set to a constant, whereas the frequency of the tremor can be controlled by the actuator. The dynamics of the experimental setup is obtained by using Newton-Euler formulation, as the elbow joint force can be measured, which will be an input to the flexure mechanism design. The experiments were conducted for three designs when they are used as a passive device or an active device.

Our contributions are design, analysis and evaluation of flexure mechanisms that can be used to compensate tremors instead of using sophisticated manipulators. Also, the performances of flexure mechanisms in passive and active modes are verified through experimental studies.

The paper is organized as follows: Section II discusses the design of flexures where the pseudo-rigid model is used to develop the mechanism. Section III shows the Finite Element (FE) simulation for the known load. In section IV, based on the designed flexure, a series of experiments were performed using the in-house developed experimental setup. The section V provides a conclusion based on the simulation and experimental results.

II. FLEXURE MECHANISM AND MODELLING

A. BASIC CONCEPT

The concept of a tremor compensation system is shown in Fig. 1, which is placed under the elbow. A mannequin model

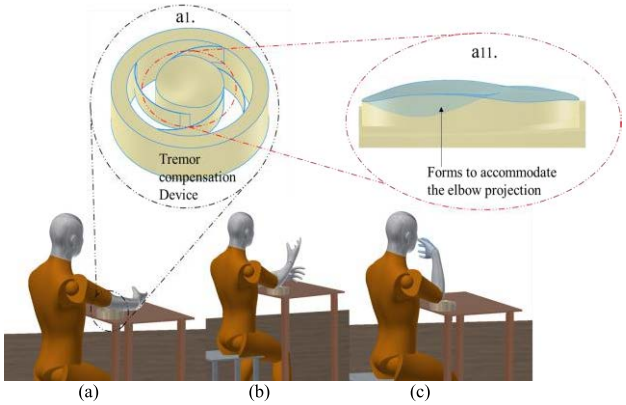

FIGURE 1. A mannequin is shown in sitting posture (a), (b), and (c) shows the different position of the arm, while having flexure mechanism tremor compensation device placed under the arm, bubble (a1) shows the flexure mechanism, and bubble (a11) shows a quadratic surface provided to rest the elbow.

is used to demonstrate the sitting posture, having a flexure mechanism at the elbow to compensate for the tremor of the arm and ease in conducting daily activity (in a sitting posture).

The tremor compensation device is based on the flexure member, connects the inner and outer platform. The outer platform will be placed on the table (grounded), whereas the inner platform will rest the elbow.

A quadratic surface (form) is shown in Fig. 1 where a_{11} is provided on the inner platform to match the contour of the human elbow joint. In general, hand tremors can be assumed as six-DOF involuntary motions generated due to the central neurogenic and/or mechanical reflex. The six-DOF curved flexure mechanism is conceptualized.

B. DESIGN OF FLEXURE MECHANISM

Three flexure mechanisms are designed as shown in Fig. 2. The inner platform (i.e., moving platform) has 6-DOF motion, whereas the outer platform (i.e., fixed platform) is grounded. Depending upon different connections, we have three configurations designated as a single strand parallel flexure mechanism, SSPFM (type-1), the multiple-strands parallel flexure mechanism, MSPFM (type-2), and multiple strands parallel and serial flexure mechanism, MSPSFM (type-3).

C. ANALYSIS OF CURVED FLEXURE MECHANISM

A curved beam flexure is considered for our design such that linear motion can be provided by straightening the curved beam. The flexure, in general, is considered as a straight member and has no initial curvature [25]. So, linear motion along the longitudinal axis is almost negligible due to axial deformation. From the geometry, the possible maximum linear motion about the transverse axis can be estimated (say ΔL_1). One of the curved flexure (say flexure-1) from SSPFM is shown in Fig. 3(a); all possible forces F_{1x}, F_{1y}, F_{1z}, and moments M_{1x}, M_{1y}, M_{1z} are marked about the X, Y, and Z-axis, respectively.

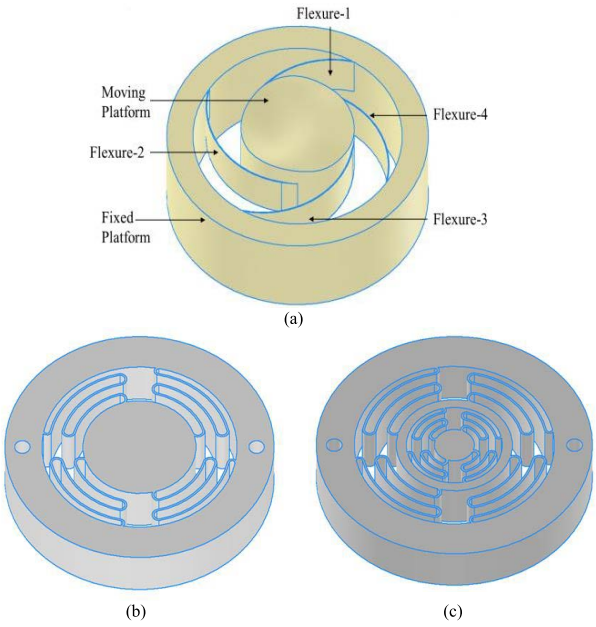

FIGURE 2. Flexure mechanisms to compensate tremor: (a) Flexure mechanism type-1: single strand parallel flexure mechanism (SSPFM), (b) Flexure mechanism type-2: multiple strands parallel flexure mechanism (MSPFM), and (c) Flexure mechanism type-3: multiple strand, parallel and serial flexure mechanism (MSPSFM).

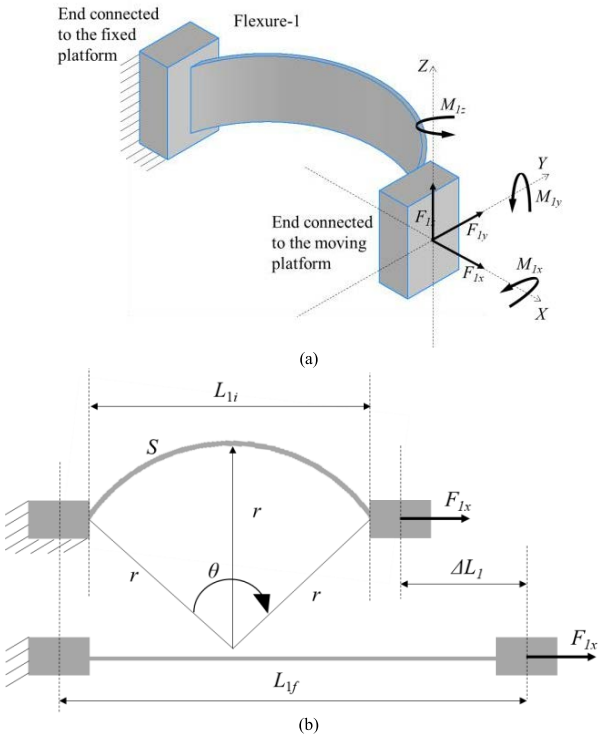

FIGURE 3. (a) Forces and moments applied at the free end on a flexure strand (b) Maximum possible deflection on the strand when force is applied.

Let the initial horizontal length of the curved flexure be L_{1i}, which has an arc length of S; angle θ suspended at the center of curvature and the radius r as curvature. If a force F_{1x} is applied to the longitudinal axis, then the curvature of the flexure will decrease, and the final longitudinal length L_{1f} may become less than or equal to S. Then, the change in length can be estimated using the geometry as expressed in (1)

$$\begin{aligned}\Delta L_1 &= L_{1f} - L_{1i} \\ &= \left(\frac{\theta}{360} 2 \times \pi \times r\right) - \left(2 \times r \times \sin\left(\frac{\theta}{2}\right)\right) \end{aligned} \quad (1)$$

The flexure is designed using Castigliano's displacement theorem. Permissible linear deflection u_i can be estimated using the total strain energy U by the force F_i on that section (say i). Similarly, angular deflection θ_i can be estimated by the total strain energy U by the moment M_i on the section (say i).

As shown in Fig. 3(b), the fully stretched flexure will be limited to deformation. The linear deflection u_{1x} along the X-axis in general can be written as in (2).

$$\begin{aligned} u_{1x} = &\frac{1}{EI}\left(\int_0^L M_{1y}\frac{\delta M_{1y}}{\delta F_{1x}}dx + \int_o^L M_{1z}\frac{\delta M_{1z}}{\delta F_{1x}}dx\right) \\ &+ \frac{1.2}{GA}\left(\int_0^L F_{1y}\frac{\delta F_{1y}}{\delta F_{1x}}dx + \int_o^L F_{1z}\frac{\delta F_{1z}}{\delta F_{1x}}dx\right) \\ &+ \frac{1}{EA}\int_0^L N_{1x}\frac{\delta F_{1x}}{\delta F_{1x}}dx + \frac{1}{GJ}\int_o^L M_{1x}\frac{\delta M_{1x}}{\delta F_{1x}}dx \end{aligned} \quad (2)$$

where F_{1x}, F_{1y}, and F_{1z} are forces and M_{1x}, M_{1y}, and M_{1z} are moments along X, Y, and Z-axis, respectively. E is the Modulus of elasticity, I is the moment of Inertia, G is the Modulus of rigidity, A is the area of cross-section.

After substituting the partial differentiation component, the expression can be further reduced.

$$u_{1x} = \frac{1}{EA} F_{1x} L_{1f} \quad (3)$$

Here the flexure length (L_{f1}) was taken as 42 *mm* as the possible maximum length to accommodate the region. The flexure thickness was taken as 0.5 *mm*, limited by the machining capability of the 3D printer (available in our lab). The force (span) exerted along the X-axis can be estimated as 12 N and discussed in section III C. Considering permissible deformation u_{x1} along the X-axis as of 0.05 *mm*, the breadth was determined as 4.39 *mm*. Thus, SSPFM (type-1) is designed.

The MSPFM (type-2) is designed by adding multiple flexure strands, which increase the mechanism's axial flexibility. In total, three strands were arranged in series (as the possible number that can be modeled within the closed region). One of the flexure lengths is equal to L_{f1}, and a gradual reduction in flexure length is by a factor of 0.25.

Additionally, MSPSFM (type-3) is designed to have parallel and serial combinations of flexure. One of the flexure lengths was taken as equal to L_{f1}, and a gradual reduction in flexure length by a factor of 0.25 was considered for the

outer ring. Similarly, the flexure for the inner ring was modeled. Based on the designed flexure mechanisms, pseudo-rigid models are developed to study the flexibility of the mechanisms and verified using the FE simulation package.

D. PSEDO-RIGID MODEL OF FLEXURE MECHANISM

The motion of the moving platform of the flexure mechanism can be estimated using a pseudo-rigid model. One of the curved flexure form, SSPFM (say flexure-1) is shown in Fig. 4. An equivalent pseudo-rigid model can be made by replacing the flexure into a rigid body having torsional spring joints [26].

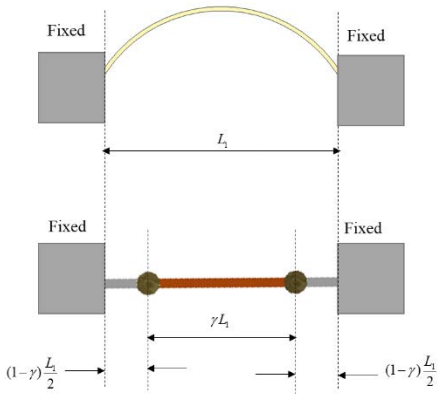

FIGURE 4. A equivalent pseudo-rigid model of a curved flexure strand.

The rigid length of the link is divided into three elements: two rigid lengths of $(1\text{-}\gamma)L_1/2$ are between the fixed support and the joint (torsional spring joint) and one rigid length of γL_1 between the two joints (torsional springs joints), where γ is the characteristic radius factor and L_1 is the initial horizontal length of the flexure-1. The stiffness (combined effect due to two torsional springs) of the link about the X, Y, and Z-axis can be expressed as in (4)-(6), respectively.

$$K_{xi} = \rho K_\theta \frac{EI_{xx}}{L_1} \tag{4}$$

$$K_{yi} = \rho K_\theta \frac{EI_{yy}}{L_1} \tag{5}$$

$$K_{zi} = \rho K_\theta \frac{EI_{zz}}{L_1} \tag{6}$$

where K_{xi} is the stiffness about the X-axis for the i^{th} flexure (i is 1 in this case), similarly K_{yi} and K_{zi} are the stiffness about the Y, and Z-axis for the i^{th} flexure (i is 1 in this case), respectively; E is the young modulus; I_{xx} is the moment of inertial about the X-axis; I_{yy} is the moment of inertial about the Y-axis; I_{zz} is the moment of inertial about the Z-axis; ρ has the value of 0.749, and K_θ has the value of 2.99 [26].

A pseudo-rigid model is used for modeling three flexure mechanisms: SSPFM (type-1), MSPFM (type-2), and MSPSFM (type-3). Based on the developed pseudo-rigid model, MATLAB simulation is conducted to determine the deflection to the applied known loads and is discussed below.

1) SSPFM (FLEXURE MECHANISM TYPE-1)

The motion of the moving platform of SSPFM is due to the elastic deformation of the curved flexures. The curved beam is equivalently represented as a straight beam having spring-loaded joints to estimate the motion. The spring stiffness for a single flexure has been expressed in (4)- (6), and the same notation is used to model for SSPFM.

Fig. 5(a) shows the SSPFM (type-1), and Fig. 5(b) shows an equivalent pseudo-rigid model, where curved links are replaced with the rigid link and torsional-springs. Local frames are attached to the base of the flexure as #F_1, #F_2, #F_3, and #F_4, and a global frame #F_E is attached to the center of the mechanism. The frames' three orthogonal axes (i.e., X, Y, and Z-axis) are represented using three colors as shown in Fig. 5(c), where the red color axis represents X-axis, the green color axis represents Y-axis, and the blue color axis represents Z-axis.

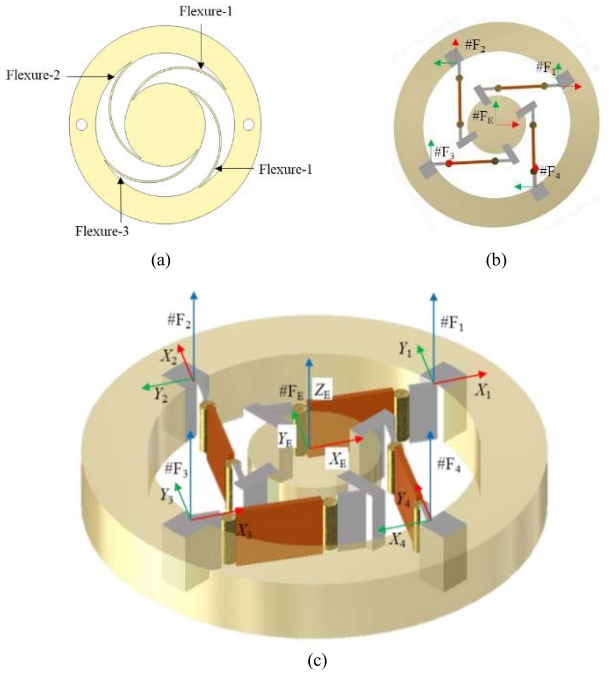

FIGURE 5. (a) A flexure mechanism type-1 (SSPFM) consisting for four curved flexure strands, (b) Top view of the Pseudo-Rigid model having frames attached, and (c) Isometric view of the Pseudo rigid model having frames attached.

The stiffness of flexure-i (where $i = 1$ to 4) about the X, Y, and Z-axis can be expressed in the inertial frame (F_E) using (4)-(6), respectively. The X, Y, and Z-axis stiffness can be expressed as in (7)- (9), respectively.

$$K_x = K_{x1} + K_{x2} + K_{x3} + K_{x4} \tag{7}$$

$$K_y = K_{y1} + K_{y2} + K_{y3} + K_{x4} \tag{8}$$

$$K_z = K_{z1} + K_{z2} + K_{z3} + K_{z4} \tag{9}$$

where K_x, K_y, and K_z is the stiffness about X, Y, and Z-axis in inertial frame (F_E), K_{xi} is the stiffness of flexure-i about the X-axis, K_{yi} is the stiffness of flexure-i about Y-axis, and K_{zi} is the stiffness of flexure-i about Z-axis.

The deflection about X, Y, and Z-axis was determined for the known forces as discussed in Section-III-C. The X, Y, and Z-axis stiffness for SSPFM was determined as 2.3 *Nmm*, 2.8 *Nmm*, and 7.8 *Nmm*, respectively. Fig. 6 shows the deflection vs. time for the flexure type-1. It shows that the maximum deformation is along the X-axis. In contrast, the Y and Z-axis have comparatively less deflection, though the X and Y-axis stiffness is almost the same and relatively lower than the Z-axis stiffness.

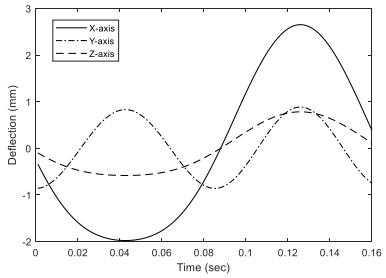

FIGURE 6. Pseudo-rigid model simulation result showing deflection vs. time when the flexure mechanism type-1 is loaded to known forces F_x, F_y and F_z.

2) MSPFM (FLEXURE MECHANISM TYPE-2)

The motion of the moving platform of MSPFM is due to the elastic deformation of the multiple curved flexures. The curved beam is equivalently represented as a rigid beam having spring-loaded joints to estimate the motion.

For MSPFM, multiple curved flexures are in series, as shown in Fig. 7. A single strand has a series of elements of varying lengths to accommodate within the curved region. The rigid length from the fixed base to the joint is represented as (1-γ_j)L_{ij}/2 (where i is the flexure number, varies from 1 to 4 and j is flexure in series, varies from 1 to 3). The length of the link between the joints is represented as $\gamma_j L_{ij}$ where γ_j is the characteristic radius factor and L_{ij} is the initial horizontal length of the curved flexure-i.

The stiffness of flexure-i is a series combination of flexure-ij. The stiffness about the X, Y, and Z-axis of each flexure-ij can be determined using (4)-(6). Once the stiffness of flexure-ij is determined, the stiffness of flexure-i can be determined using the spring series equation and is expressed in (10)-(12).

$$\frac{1}{K_{1x}} = \frac{1}{K_{x11}} + \frac{1}{K_{x12}} + \frac{1}{K_{x13}} \tag{10}$$

$$\frac{1}{K_{1y}} = \frac{1}{K_{y11}} + \frac{1}{K_{y12}} + \frac{1}{K_{y13}} \tag{11}$$

$$\frac{1}{K_{1z}} = \frac{1}{K_{z11}} + \frac{1}{K_{z12}} + \frac{1}{K_{z13}} \tag{12}$$

where K_{x11}, K_{x12}, and K_{x13}, are the X-axis stiffness of each flexure-1j of the flexure-1, K_{y11}, K_{y12}, and K_{y13} are the Y-axis stiffness of each flexure-1j of the flexure-1, and K_{z11}, K_{z12}, and K_{z13} are the Z-axis stiffness of each flexure-1j of

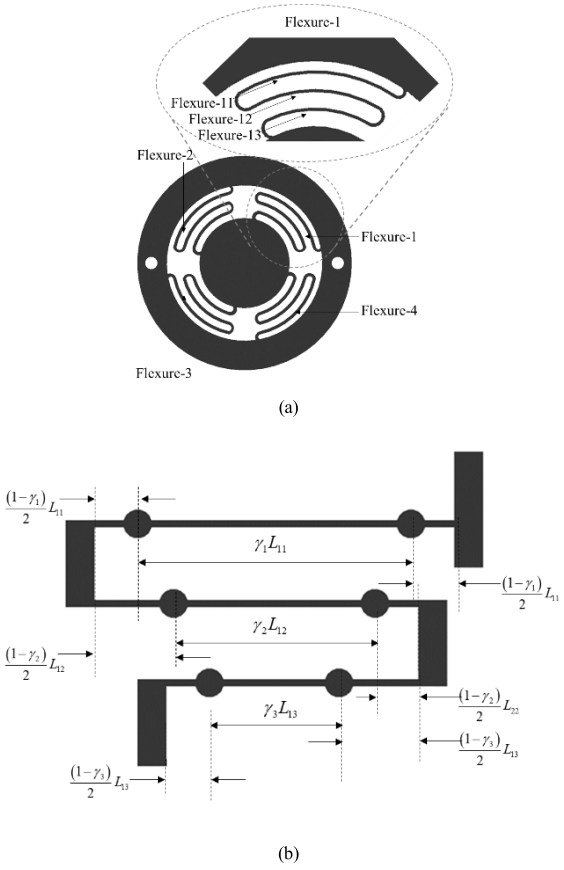

FIGURE 7. (a) Flexure mechanism type-2 (MSPFM) having curved flexure in series (b) Equivalent pseudo-rigid model.

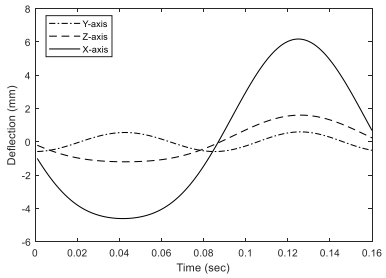

FIGURE 8. The pseudo-rigid model simulation result showing deflection vs. time when the flexure mechanism type-2 is loaded to known forces F_x, F_y, and F_z.

the flexure-1. Stiffness's of the MSPFM can be obtained in inertial frame (F_E).

The X, Y, and Z-axis stiffness can be expressed as in (10)-(12). The X, Y, and Z-axis stiffness for MSPFM was determined as 0.98 *Nmm*, 4.14 *Nmm*, and 3.8 *Nmm*, respectively. The deflection about the X, Y, and Z-axis was determined for the known forces as discussed in Section-III-C. Fig. 8 shows the deflection vs. time for the flexure type-2. The plot shows the maximum deformation along the X-axis. In contrast, the Y and Z-axis have comparatively less deflection, though the stiffness about Y, and Z-axis is almost the same and relatively higher than the X-axis stiffness.

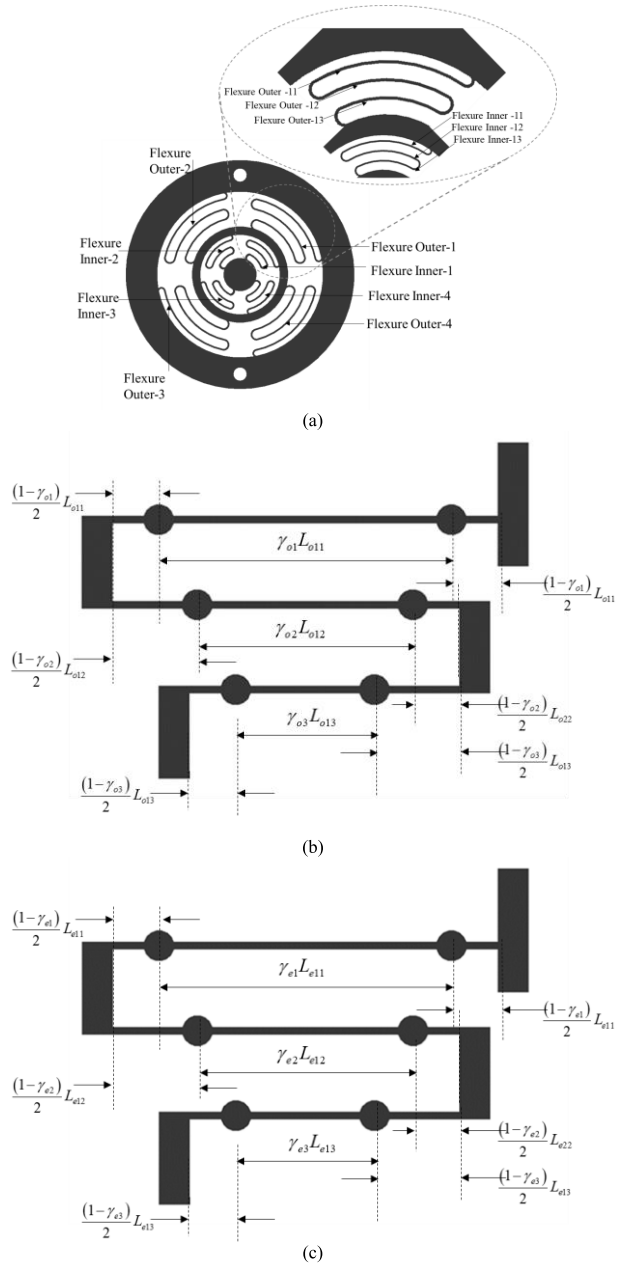

FIGURE 9. (a) Flexure mechanism type-3 (MSPSFM) having curved flexure in series and parallel (b) Equivalent pseudo-rigid model for the outer flexure (c) Equivalent pseudo-rigid model for the inner flexure.

3) MSPSFM (FLEXURE MECHANISM TYPE-3)

The motion of the moving platform of MSPSFM is due to the elastic deformation of the multiple parallel-series curved flexures, as shown in Fig. 9(a). The curved beam is equivalently represented as a rigid beam having spring-loaded joints to estimate the motion. A single strand in the inner and outer flexure has a series of flexures of varying lengths to accommodate the curved region. The rigid length from the fixed base to the joint is represented as $(1\text{-}\gamma_{ej})L_{eij}/2$ (where e is for inner flexure, i is the flexure number that varies from 1 to 4, and j is flexure in series that varies from 1 to 3) where γ_{ej} is the characteristic radius factor and L_{eij} is the initial horizontal length of the curved flexure-i.

The length of the link between the joints is represented as $\gamma_{ej}L_{eij}$. Similarly, for the outer flexures, the rigid length from the fixed base to the joint is represented as $(1\text{-}\gamma_{oj})$ $L_{oij}/2$ (where o is for outer flexure, i is the flexure number, varies from 1 to 4,and j is flexure in series, varies from 1 to 3) where γ_{oj} is the characteristic radius factor, and L_{oij} is the initial horizontal length of the curved flexure-i. The length of the link between the joints is represented as $\gamma_{oj}L_{oij}$.

The stiffness of flexure-outer-i and flexure inner-i is from series combinations of flexure-oij and flexure-eij. The stiffness about the X, Y, and Z-axis of each flexure can be determined using (4)-(6). Once the stiffness of flexure-oij and flexure-eij are determined, the stiffness of flexure-ei can be determined using the spring series equation and expressed in (10)-(12).

The X, Y, and Z-axis stiffness can be expressed as in (7)-(9). The X, Y, and Z-axis stiffness for MSPSFM was determined as 0.96 *Nmm*, 4.01 *Nmm*, and 3.7 *Nmm*, respectively. The deflection about the X, Y, and Z-axis was determined for the known forces as discussed in Section-III-C. Fig. 10 shows the deflection vs. time for the flexure type-3. It shows the maximum deformation along the X-axis. In contrast, the Y and Z-axis have comparatively less deflection, though the stiffness about the Y and Z-axis is almost the same and relatively higher than the X-axis stiffness.

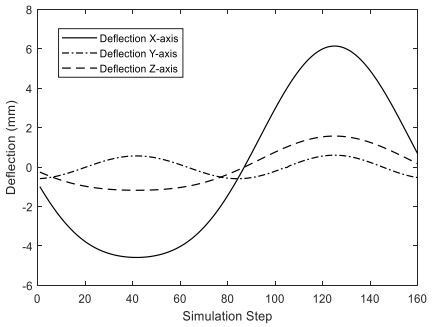

FIGURE 10. Pseudo-rigid model simulation result showing deflection vs. time plot when the flexure mechanism type-3 is loaded to a known a forces F_x, F_y and F_z about X, Y, and Z -axis.

4) SUMMARY OF STIFFNESS OF FLEXURE MECHANISM

The stiffness of the flexure mechanism has been summarized in Table 1. For SSPFM (type-1), the X and Z-axis stiffness were higher than the other two flexure mechanisms. MSPFM (type-2) has higher stiffness about the Y-axis as compared to SSPFM (type-1) and almost the same stiffness as compared to MSPSFM (type-3). Based on the stiffness model, MSPFM (type-2) and MSPSFM (type-3) have the similar performance, whereas SSPFM (type-1) has higher stiffness.

TABLE 1. Stiffness of the flexure mechanism type-1 (SSPFM), type-2 (MSPFM) and type-3 (MSPSFM).

S. No	Flexure Mechanism	Direction	Values (*Nmm*)
1	Type-1	*X*-axis	2.3
		Y-axis	2.8
		Z-axis	7.8
2	Type-2	*X*-axis	0.98
		Y-axis	4.14
		Z-axis	3.8
3	Type-3	*X*-axis	0.96
		Y-axis	4.01
		Z-axis	3.77

III. SIMULATION STUDIES

A. FINITE ELEMENT SIMULATION

An ANSYS simulation package was used to simulate the flexure mechanism for the known elbow loads. The model was imported to the design modeler. The material property of ABS material was used, and the mesh of hex-dominated elements was used. Boundary conditions were applied on the outer platform as a fixed type. The inner platform was loaded with the known force and moment values determined in Section-III-C. The load was stepped into 160 intervals. The load data from the MATLAB of 160-time intervals were imported to the ANSYS mechanical modeler window.

The dynamic analysis in Section-III-C only gives three load components (i.e., force about X-axis, Y-axis, and moments about Z-axis: this is due to a 2-DOF model). But other three loads were assumed for six different simulations (i.e., forces and moments about X, Y, and Z-axis). Hence, the force along the Z-axis was considered equal to the force along the X-axis, and the moments along the X, Y-axis was considered equal to the moment along the Z-axis. One load (i.e., force or moment) was applied at one instance, and deflection was recorded. The simulation for three different types of flexure was conducted for the six different types of loads (three forces and three moments), and the contour plots for the deflection are shown in Fig. 11. For the forces/moments applied on SSPFM (type-1), the deformation contour plots are shown in Fig. 11(a). The force along the X, Y, and Z-axis as applied for simulation is shown in Fig. 11(a) from top right to left. For the moments along the X, Y, and Z-axis as applied for simulation is shown in Fig. 11(a) from bottom right to left. The figure typically shows the deformed shape and the gradient plot of the flexure when loaded to forces and moments.

Similarly, the deformation contour plots for the forces/moments applied on MSPFM (type-2) are shown in Fig. 11(b) and for MSPSFM (type-3) in Fig. 11(c), respectively.

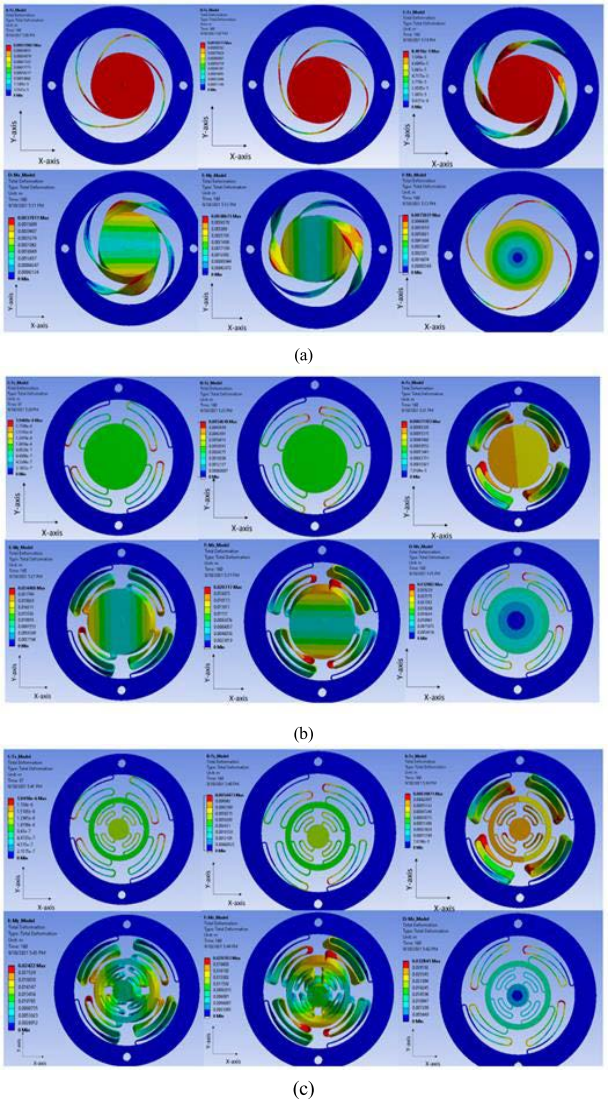

FIGURE 11. The deformation contour plot when a force or moment is applied on (a) Flexure mechanism type-1, when force along *X*, *Y*, *Z* -axis is applied from top right to left and when moments along *X*, *Y*, *Z* -axis is applied from bottom right to left, (b) Flexure mechanism type-2, when force or moment are applied in the same sequence as in the above case. (c) Flexure mechanism type-3, when force or moment is applied in the same sequence as in the above case.

B. DEFLECTION ANALYSIS

The finite element (FE) simulation was conducted for three different models for six separate load instances based on the above methods.

1) SSPFM (FLEXURE MECHANISM TYPE-1)

Using the FE simulation results for SSPFM (type-1), the deflections due to forces (along X, Y, Z-axis) and moments (along X, Y, Z-axis) are shown in Fig. 12 (a), and (b), respectively.

Higher deflection (max. of 2.8 *mm* and min. of -2.16 *mm*) was observed for the force along the X-axis due to the magnitude of load being much higher, and the system has much lower stiffness along the X-axis. The

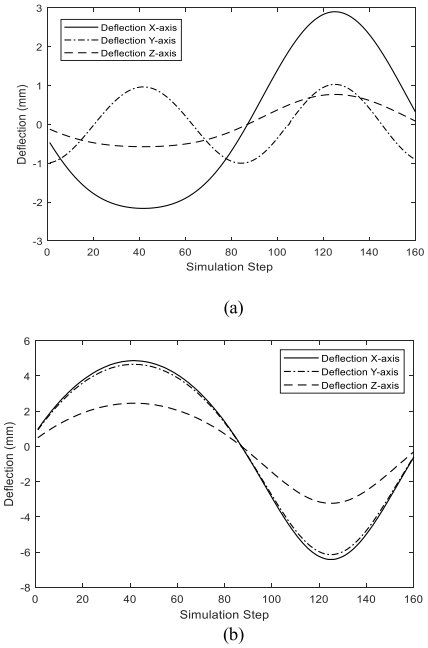

FIGURE 12. FE simulation result showing the deflection value when (a) forces are applied on flexure mechanism type-1, (b) moments are applied on flexure mechanism type-1.

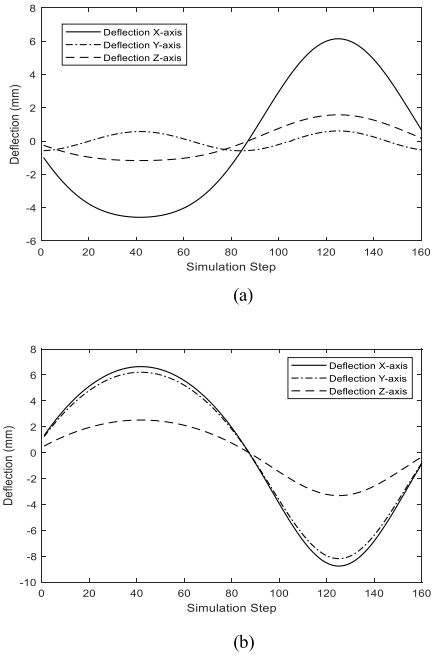

FIGURE 13. FE simulation result showing the deflection value when (a) forces are applied on flexure mechanism type-2, (b) Moments are applied on flexure mechanism type-2.

same nature of force was applied along the Z-axis, but the deflections (max. of 0.76 *mm* and min. of -0.57 *mm*) are relatively low due to high stiffness along this axis, and the maximum and minimum deflections were recorded as 1.02 *mm* and -0.96 *mm* for the case of force along the Y-axis. For the moment, higher deflection (max. of 4.87 *mm* and min. of -6.42 *mm*) was observed along the X-axis, which is also a close matching deflection (max. of 4.66 *mm* and min. of -6.15 *mm*) for the moment along the Y-axis, the values are very relative due to the symmetry in structure. The moment along the Z-axis, the maximum and minimum deflections were recorded as 2.45 *mm* and -3.23 *mm*, respectively.

2) MSPFM (FLEXURE MECHANISM TYPE-2)

For MSPFM (flexure type-2), the deflections due to forces (along X, Y, Z-axis) deflection due to moment (along X, Y, Z-axis) are shown in Fig. 13, where higher deflection (max. of 6.17 *mm* and min. of -4.61*mm*) was observed for the force along the X-axis. Whereas the exact nature of force was applied along the Z-axis, but the deflections (max. of 1.6 *mm* and min. of -1.19 *mm*) are relatively low due to high stiffness along this axis. For the case of force along the Y-axis, the maximum and minimum deflections were recorded as 0.57 *mm* and -0.58 *mm*.

For the moment, higher deflection (max. of 7.8 *mm* and min. of -10.34 *mm*) was observed along the X-axis, which is also a close matching deflection (max. of 7.42 *mm* and min. of -9.8 *mm*) with the moment along the Y-axis, the values are very close due to the symmetry in structure.

For the case of the moment along the Z-axis, maximum and minimum deflections were recorded as 3.14 *mm* and -4.15 *mm*, respectively.

3) MSPSFM (FLEXURE MECHANISM TYPE-3)

For MSPSFM (flexure type-3), the deflections are plotted in Fig. 14. Higher deflection (max. of 6.13 *mm* and min. of -4.5 *mm*) was observed for the force along the X-axis. Due to high stiffness along the Z axis, the deflections (max. of 1.60 *mm* and min. of -1.19 *mm*) are relatively low and the maximum and minimum deflection were recorded as 0.56 *mm* and -0.56 *mm* for the force along the Y-axis.

For the moment, higher deflection (max. of 6.63 *mm* and min. of -8.75 *mm*) was observed along the X-axis, also a close matching deflection (max. of 6.19 *mm* and min. of -8.18 *mm*) with the moment along the Y-axis, the values are very close due to the symmetrical structure. For the case of the moment along the Z-axis, the maximum and minimum deflections were recorded as 2.5 *mm* and -3.32 *mm* respectively.

C. KINEMATICS AND DYNAMICS OF TREMOR SETUP

For designing the flexure mechanism, forces and moments at the elbow joint were required. The kinematic and dynamic models are developed for the 2-DOF setup as shown in Fig. 15. The 2-DOF mechanism has two revolute joints equivalent to the shoulder and elbows joint, and the free end is connected to the tremor generator system.

For the kinematic modeling, Denavit-Hartenberg notation is used. The free effector position (x_{fe}, y_{fe}) can be mapped to

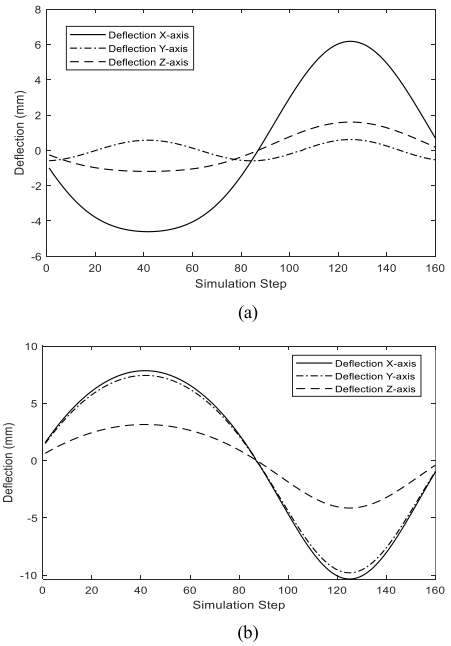

FIGURE 14. FE Simulation result showing the deflection value when (a) forces are applied on flexure mechanism type-3, (b) Moments are applied on flexure mechanism type-3.

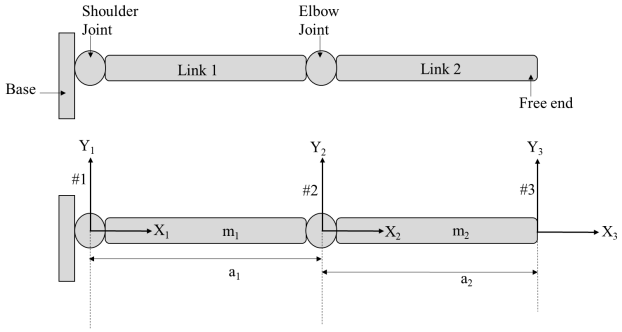

FIGURE 15. Skeleton model of the two link serial chain mechanism.

the inertial frame {#1} by (13).

$$\left.\begin{aligned} x_{fe} &= a_1 \cos\theta_1 + a_2 \cos(\theta_1 + \theta_2) \\ x_{fe} &= a_1 \sin\theta_1 + a_2 \sin(\theta_1 + \theta_2) \end{aligned}\right\} \tag{13}$$

where a_1 and a_2 are the link length and θ_1 and θ_2 are shoulder and elbow joint angles, respectively. The joint velocity $(\dot{\theta}_1,\ \dot{\theta}_2)$ and joint acceleration $(\ddot{\theta}_1,\ \ddot{\theta}_2)$ determined in the inertial frame can be mapped by performing the first and second derivatives of the displacement (13).

The Newton-Euler formulation is used to model the joint forces and moment. The dynamics equations are shown as

$$\begin{aligned} F_{El\_x} = m_2(-a_1\dot{\theta}_1^2 - \frac{a_2}{2}(\sin\theta_2(\ddot{\theta}_1 + \ddot{\theta}_2) \\ + \cos\theta_2(\dot{\theta}_1 + \dot{\theta}_2)^2)) \end{aligned} \tag{14}$$

$$\begin{aligned} F_{El\_y} = m_2(-a_1\ddot{\theta}_1 + \frac{a_2}{2}\cos\theta_2(\ddot{\theta}_1 + \ddot{\theta}_2) \\ - \sin\theta_2(\dot{\theta}_1 + \dot{\theta}_2)^2) \end{aligned} \tag{15}$$

$$\begin{aligned} n_{El\_z} = -\frac{a_2}{2}\sin\theta_2 \times F_{12x} + \frac{a_2}{2}\cos\theta_2 \times F_{12y} \\ + m_2\frac{a_2^2}{12}(\ddot{\theta}_1 + \ddot{\theta}_2) \end{aligned} \tag{16}$$

where F_{El_x} is the force on the elbow joint along the X-axis, F_{El_y} is the force on the elbow joint along the Y-axis, n_{El_z} is the moment at the elbow joint along the Z-axis, a_1 and a_2 are the link length of the upper and lower arm, m_1 and m_2 are the mass of upper and lower arm.

For the kinematic and dynamic study of hand tremors, the link parameters were considered as listed in Table 2.

TABLE 2. Link parameters for the two link experimental setup.

S. No	Arm	Nomenclature	Values
1	Link-1 (Upper arm)	length (a_1)	0.156 m
		Mass (m_1)	0.19 kg
2	Link-2 (Lower arm)	Length (a_2)	0.143 m
		Mass (m_2)	0.04 kg

The physiological tremor has an amplitude of 0.14 m and frequency of 6-9 Hz [14]. For our study, the amplitude was reduced to half and kept the frequency same as the experimental setup is nearly designed to the half the size of human arm anthropometry.

The reduced hand tremor data were given to the kinematic model as free end motion. The inverse kinematics was conducted to determine the joint tremor angles (using (13)), the time derivative and double derivative of joint angles were evaluated to determine the joint velocity and joint acceleration, respectively.

The inverse dynamics was performed to determine the joint forces and moments. Fig. 16(a) shows the elbow forces, and Fig. 16(b) shows the elbow moments. Forces along the X-axis have maximum and minimum values of 6.1 and -4.6 N, forces along the Y-axis have maximum and minimum values of 2.4 and -2.4 N, and moments along the Z-axis have maximum and minimum values of 3.6 and -4.69 Nm, respectively.

D. SUMMARY OF SIMULATION RESULTS

The three flexure mechanisms were simulated, and the ANSYS results show a close match to the pseudo-rigid model. For SSPFM (type-1), Fig. 6 and Fig. 12(a) show the deflection plot when forces are applied along the X, Y, and Z-axis. Similarly, for MSPFM (type-2), Fig. 8 and 13 (a) show the deflection plot when forces are applied along the X, Y, and Z-axis. Similarly, for MSPSFM (type-3), Fig. 10 and 14(a) show the deflection plot when forces are applied along the X, Y, and Z-axis. A comparison result in Table-3 is drawn based on the deflection plot, maximum and minimum values of the deflection (mm) are plotted when the known forces (N) are applied for the cases: when the model is a pseudo-rigid model, finite element model for flexure mechanism type-1, 2 and 3. Thus, the data shown in Table 3 clearly

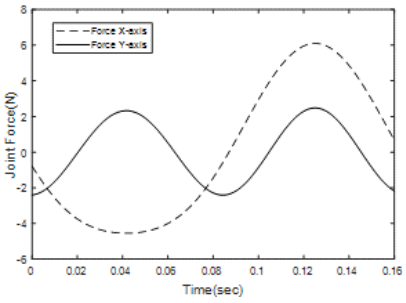

(a) **Forces along *X*-axis and *Y*-axis**

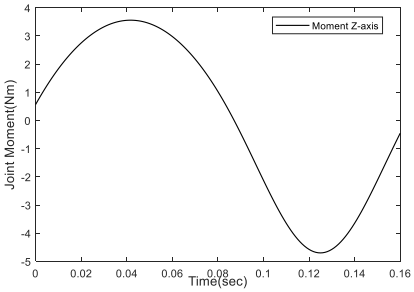

(b) **Moment along *Z*-axis**

FIGURE 16. The simulation results for the elbow joint.

show that pseudo-rigid model data have close correlation with the FE simulation data.

IV. EXPERIMENTAL STUDIES

A. EXPERIMENTAL SETUP

1) OVERALL SYSTEM

For conducting the experiment, an experimental setup is designed as shown in Fig. 17. It consists of a two-link-planar robot representing the human hand, a tremor generator system, and active/passive tremor compensation systems.

A two-link mechanism is modeled, consisting of springs at the joints. Springs are attached to the joints such that tremors at the free end of the link are transferred to the robot's elbow and shoulder joint. Gyroscope sensors are placed on both the ends (fixed and free) of the robot to record the tremor present.

A tremor compensation system consists of a flexure mechanism (i.e., either flexure type-1, 2 or 3), a flexure mechanism holder, and an active tremor compensator mechanism. The flexure mechanism is placed to the elbow, and positioning adjustments are taken care by the holder, which is grounded. An active tremor compensation system is designed and coupled to the flexure mechanism. Such that it generates an equivalent compensation tremor on the (passive) flexure mechanism such that the tremor can be further compensated.

For the active tremor compensation, a one-DOF mechanism is modeled and is coupled with the passive flexure system, as shown in Fig. 18. The active tremor compensation system is synthesized using a slider-crank mechanism. It is a replica of a tremor generator (discussed below) and designed such that the same nature of compensation tremor can be generated but with a phase shift.

TABLE 3. Maximum and minimum of forces obtained for the flexure mechanism type-1, 2, and 3, designed for tremor compensation.

Model	Flexure Mechanism	Force axis	Minimum deflection (*mm*)	Maximum deflection (*mm*)
Pseudo-rigid	Type-1	*X*-axis	-1.97	2.65
		Y-axis	-0.859	0.829
		Z-axis	-0.583	0.779
	Type-2	*X*-axis	-4.6052	6.171
		Y-axis	-0.558	0.042
		Z-axis	-1.197	1.603
	Type-3	*X*-axis	-4.608	6.608
		Y-axis	-0.569	0.561
		Z-axis	-1.195	1.605
Finite Element	Type-1	*X*-axis	-2.163	2.89
		Y-axis	-1	0.96
		Z-axis	-0.57	0.76
	Type-2	*X*-axis	-4.608	6.171
		Y-axis	-0.581	0.572
		Z-axis	-1.193	1.599
	Type-3	*X*-axis	-4.57	6.142
		Y-axis	-0.575	0.563
		Z-axis	-1.174	1.568

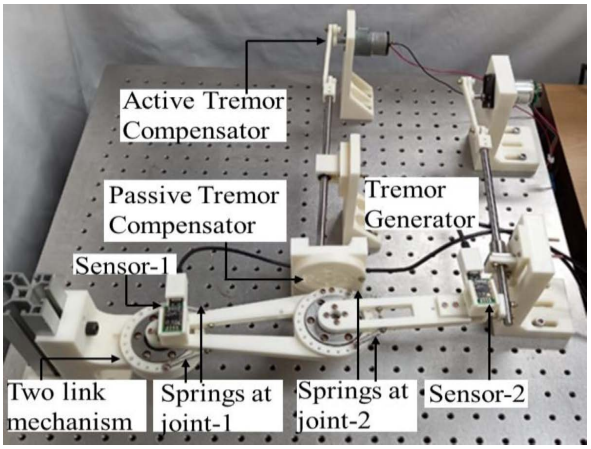

FIGURE 17. An experimental setup to conduct a series of experiment using flexure type-1, type-2, type-3 when it is loaded passively and actively.

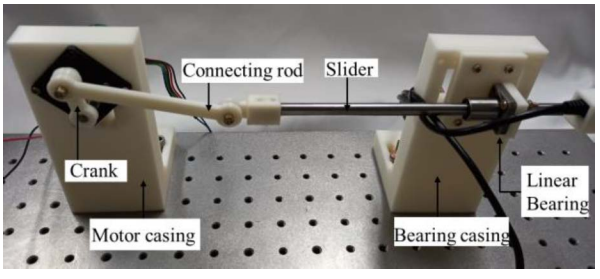

FIGURE 18. A slider crank mechanism to generate tremor of desired amplitude and frequency.

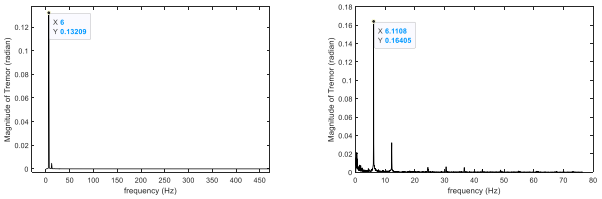

FIGURE 19. The amplitude vs. frequency plot: (a) The simulation model, and (b) The experimental setup.

2) TREMOR GENERATOR

A slider-crank mechanism is designed for generating tremor at the free end of the two-link robot, as shown in Fig. 18. The mechanism consists of a slider oscillating at the desired frequency and has a constant amplitude. The slider-crank mechanism was selected after many design iterations.

The tremor generator system consists of a crank, a connecting rod and a slider, as shown in Fig. 18. The crank is connected to a DC motor, whose rotation (frequency) can be controlled by the DC power supply, and the amplitude is equal to twice the crank length. The whole mechanism is elevated and supported by casing such that it can be attached to the free end of the two-link robot.

B. EXPERIMENTAL RESULTS

1) COMPARISON BETWEEN SIMULATION AND EXPERIMENT

A series of experiments were conducted using the two-DOF tremor generator manipulator. A constant amplitude tremor of (3.5 *cm*) having a frequency of 6 *Hz*, was generated. The tremor generated by the mechanism was recorded by the accelerometer and was also verified with the simulation data (based on the inverse kinematic). The tremor data generated at the shoulder and simulated data are shown in Fig. 19. The simulated model has the frequency of 6 *Hz* and amplitude of 7.5° (0.132 *radians*) at the shoulder joint when the free end is acted by a tremor of frequency 6 *Hz* and amplitude of 3.5*cm* (for 14 *cm* [2] as the oscillation length, the reduced amplitude is 3.5 *cm*). The experimental setup has a recoded frequency of 6.11 *Hz* and an amplitude of 9.39° (or 0.164 *radians*).

2) PASSIVE FLEXURE MECHANISM PERFORMANCE

In the first experiment, SSPFM (type-1) was placed at the elbow joint, and the two-DOF robot was activated at the set frequency of 6 *Hz* with an amplitude of 3.5 *cm*. The accelerometer mounted on the shoulder was activated, and the data were acquired. Similar experiments were performed for the other two flexure mechanisms. The acquired data are shown in Fig. 20.

For the first set of experiments, when no-flexure was placed, the tremor was recorded as 6.13 *Hz* and 0.164 *radians*. The data were recorded as 5.7 *Hz* and 0.020 *radians* for SSPFM (type-1), 5.8 *Hz* and 0.0377 *radians* for MSPFM (type-2), and finally, 6.039 *Hz* and 0.0365 *radians* for MSPSFM (type-3), respectively.

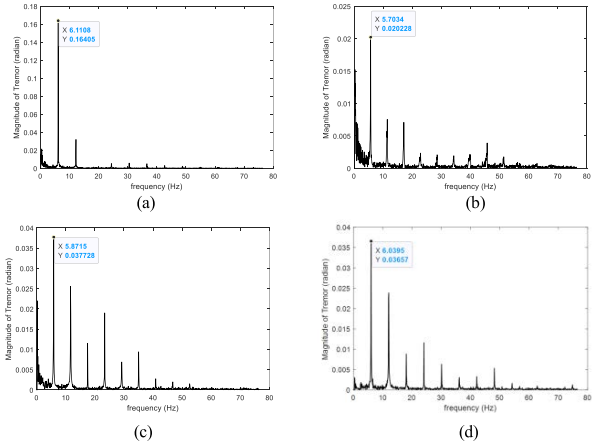

FIGURE 20. For the passive flexure study, FFT of the shoulder accelerometer data when (a) no-flexure mechanism is applied, (b) flexure mechanism type-1 is applied, (c) flexure mechanism type-2 is applied, (d) flexure mechanism type-3 is applied.

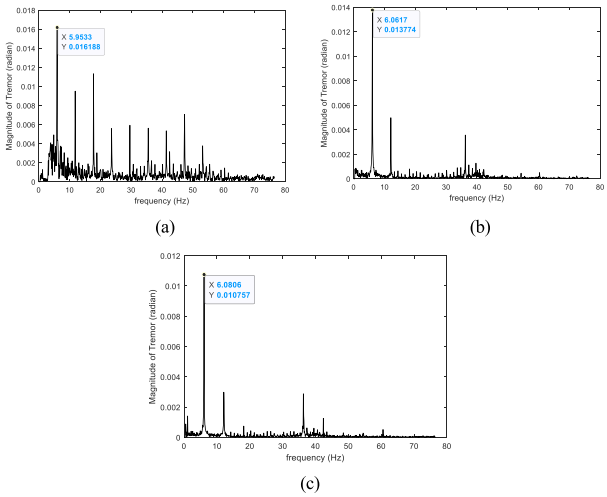

FIGURE 21. For the active flexure study, FFT of the shoulder accelerometer data (a) Flexure mechanism type-1 is applied, (b) Flexure mechanism type-2 is applied, (c) Flexure mechanism type-3 is applied.

3) ACTIVE FLEXURE MECHANISM PERFORMANCE

Another set of experiments was conducted when an active tremor compensation system was coupled with the flexure mechanisms (Type-1, 2, and 3 at a time). In the first experiment, SSPFM (type-1) coupled with a tremor compensation system was placed at the elbow joint, and the two-DOF robot was activated at the set frequency of 6 *Hz* with an amplitude of 3.5 *cm*.

The acquired data for active flexure mechanism performance are shown in Fig. 21. The tremor was recorded as 5.9 *Hz* and 0.016 *radians* for SSPFM (type-1), 6.06 *Hz*, and 0.0137 *radians* for MSPFM (type-2), and finally 6.08 *Hz* and 0.0107 *radians* for MSPSFM (type-3), respectively.

C. SUMMARY OF EXPERIMENTAL RESULTS

Table 4 compares the experimental results for the cases where the flexure mechanism is used as a passive and active device.

TABLE 4. A comparison for passive and active cases.

Experiment Type	Flexure Mechanism	Amplitude (radian)	Frequency (Hz)
	No Flexure	0.164	6.1
Passive	Type-1	**0.0202**	5.7
	Type-2	0.0377	5.8
	Type-3	0.0365	6.0
Active	Type-1	0.0162	5.9
	Type-2	0.0137	6.0
	Type-3	**0.0107**	6.0

The result shows that SSPFM (type-1) is desirable as a passive system. It compensates 87% of the tremor compared to the other two flexure mechanisms, which compensate approximately 77% and 78% of tremor. At the same time, MSPSFM (type-3) is desirable as an active tremor compensation system as it compensates 93% of the tremor compared to the other two flexure mechanisms, which compensated 90% and 91% of the tremor.

V. CONCLUSION

This paper presented three flexure-based tremor isolation devices for minimizing the effect of physiological hand tremors at the joint level. Pseudo-rigid models were developed for these flexure mechanisms and their deformations were simulated. It was found that the pseudo-rigid model has a close correlation with the FE simulation results. The stiffness of the flexure mechanism was determined using the pseudo-rigid model and the corresponding flexure mechanisms were fabricated using ABS material. The flexure mechanisms were tested on the two-link mechanism coupled with a tremor generating system. MSPSFM (type-3) is more desirable when the compensation is the active mode, whereas SSPFM (type-1) is more desirable when the compensation is the passive mode. Thus, the flexure mechanism as a tabletop device is suitable to compensate for the tremor. The present study demonstrates a method to compensate for the hand tremor using the elbow as the base. This method is desirable as one can perform all possible tasks in sitting posture without changing the compensation instrumentation while earlier models are restricted to activity.

REFERENCES

[1] W. J. Friedlander, "Characteristics of postural tremor in normal and in various abnormal states," *Neurology*, vol. 6, no. 10, p. 716, 1956, doi: 10.1212/WNL.6.10.716.

[2] A. M. Halliday and J. W. T. Redfearn, "An analysis of the frequencies of finger tremor in healthy subjects," *J. Physiol.*, vol. 134, no. 3, pp. 600–611, Dec. 1956.

[3] J. H. McAuley and C. D. Marsden, "Physiological and pathological tremors and rhythmic central motor control," *Brain*, vol. 123, no. 8, pp. 1545–1567, Aug. 2000.

[4] R. J. Elbie, "Mechanism of physiological tremor and relationship to essential tremor," in *Handbook of Tremor Disorders*. 1995, pp. 51–62.

[5] G. Deuschl, P. Krack, M. Lauk, and J. Timmer, "Clinical neurophysiology of tremor," *J. Clin. Neurophysiol.*, vol. 13, no. 2, pp. 110–121, 1996.

[6] A. I. Tröster, R. Pahwa, J. A. Fields, C. M. Tanner, and K. E. Lyons, "Quality of life in essential tremor questionnaire (QUEST): Development and initial validation," *Parkinsonism Rel. Disorders*, vol. 11, no. 6, pp. 367–373, Sep. 2005.

[7] D. Lorenz, D. Schwieger, H. Moises, and G. Deuschl, "Quality of life and personality in essential tremor patients," *Movement Disorders*, vol. 21, no. 8, pp. 1114–1118, 2006.

[8] D. A. Lenrow and C. W. Slipman, "Neuromuscular function and disease: Basic, clinical, and electrodiagnostic aspects, William F. Brown, Charles F. Bolton and Michael J. Aminoff, editors, WB saunders, 2002," *Spine J.*, vol. 4, no. 1, p. 123, Jan. 2004.

[9] G. Deuschl and R. J. Elble, "The pathophysiology of essential tremor," *Neurology*, vol. 54, no. 11, pp. S14–S20, 2000.

[10] R. J. Elble, "Central mechanisms of tremor," *J. Clin. Neurophysiol.*, vol. 13, no. 2, pp. 133–144, Mar. 1996.

[11] J. Groß, L. Timmermann, and J. Kujala, "The neural basis of intermittent motor control in humans," *Proc. Nat. Acad. Sci. USA*, vol. 99, no. 4, pp. 2299–2302, 2002.

[12] R. F. Dallapiazza, D. J. Lee, P. De Vloo, A. Fomenko, C. Hamani, M. Hodaie, S. K. Kalia, A. Fasano, and A. M. Lozano, "Outcomes from stereotactic surgery for essential tremor," *J. Neurol., Neurosurg. Psychiatry*, vol. 90, no. 4, pp. 474–482, Apr. 2019.

[13] M. Fischer, M. Schraufstetter, C. Richter, F. Irlinger, and T. C. Lueth, "Tremor compensation by use of a mechatronic cup holder," in *Proc. 4th Int. ICST Conf. Pervasive Comput. Technol. Healthcare*, 2010, pp. 1–8, doi: 10.4108/ICST.PERVASIVEHEALTH2010.8885.

[14] D. Chang, G. Min Gu, and J. Kim, "Design of a novel tremor suppression device using a linear delta manipulator for micromanipulation," in *Proc. IEEE/RSJ Int. Conf. Intell. Robots Syst.*, Nov. 2013, pp. 413–418.

[15] S. Tatinati, K. Nazarpour, W. T. Ang, and K. C. Veluvolu, "Multidimensional modeling of physiological tremor for active compensation in handheld surgical robotics," *IEEE Trans. Ind. Electron.*, vol. 64, no. 2, pp. 1645–1655, Feb. 2017, doi: 10.1109/TIE.2016.2597119.

[16] C. N. Riviere, R. S. Rader, and N. V. Thakor, "Adaptive cancelling of physiological tremor for improved precision in microsurgery," *IEEE Trans. Biomed. Eng.*, vol. 45, no. 7, pp. 839–846, Jul. 1998.

[17] I. W. Hunter, T. D. Doukoglou, S. R. Lafontaine, P. G. Charette, L. A. Jones, M. A. Sagar, G. D. Mallinson, and P. J. Hunter, "A teleoperated microsurgical robot and associated virtual environment for eye surgery," *Presence: Teleoperators Virtual Environments*, vol. 2, no. 4, pp. 265–280, Jan. 1993.

[18] Y. S. Kwoh, J. Hou, E. A. Jonckheere, and S. Hayati, "A robot with improved absolute positioning accuracy for CT guided stereotactic brain surgery," *IEEE Trans. Biomed. Eng.*, vol. 35, no. 2, pp. 153–160, Feb. 1988.

[19] M. Patkin, "Ergonomics applied to the practice of microsurgery," *ANZ J. Surg.*, vol. 47, no. 3, pp. 320–329, Jun. 1977.

[20] H. J. Nagarsheth, P. V. Savsani, and M. A. Patel, "Modeling and dynamics of human arm," in *Proc. IEEE Int. Conf. Autom. Sci. Eng.*, Aug. 2008, pp. 924–928, doi: 10.1109/COASE.2008.4626407.

[21] R. Ramanathan, S. P. Eberhardt, T. Rahman, W. Sample, R. Seliktar, and M. Alexander, "Analysis of arm trajectories of everyday tasks for the development of an upper-limb orthosis," *IEEE Trans. Rehabil. Eng.*, vol. 8, no. 1, pp. 60–70, Mar. 2000.

[22] R. F. Kirsch, A. M. Acosta, E. J. Perreault, and M. W. Keith, "Measurement of isometric elbow and shoulder moments: Position-dependent strength of posterior deltoid-to-triceps muscle tendon transfer in tetraplegia," *IEEE Trans. Rehabil. Eng.*, vol. 4, no. 4, pp. 403–409, Dec. 1996.

[23] T. Kodek and M. Munih, "An analysis of static and dynamic joint torques in elbow flexion-extension movements," *Simul. Model. Pract. Theory*, vol. 11, nos. 3–4, pp. 297–311, Jul. 2003.

[24] H. J. Nagarsheth, S. V. Surve, and M. A. Patel, "Computer simulation of dynamics of human leg," in *Proc. IEEE Int. Conf. Autom. Sci. Eng.*, Sep. 2007, pp. 249–254.

[25] M. Zubair, Y. J. Choi, B. Suthar, and S. Jung, "Vibration suppression mechanism for foldable robot arm for drones," in *Proc. 18th Int. Conf. Ubiquitous Robots (UR)*, Jul. 2021, pp. 119–123.

[26] L. L. Howell, "Compliant mechanisms," in *21st Century Kinematics*. London, U.K.: Springer, 2013, pp. 189–216.